

# Interface between Lithium Metal and Garnet Electrolyte: Recent Progress and Perspective

Jin Wang<sup>+, [a, b]</sup>, Gang Huang<sup>+, [c]</sup> and Xin-Bo Zhang<sup>\*, [a]</sup>

Garnet electrolytes (GEs) with high ion conductivity, excellent stability against lithium metal (LM) as well as wide electrochemical potential window are attracting increasing interest as they have the potential to enable all-solid-state Li metal batteries (ASSLMBs). However, GEs-based ASSLMBs deeply suffer from daunting problems such as high resistance, fast

short circuit, and rapid performance degradation, which can be largely attributed to unsatisfactory LM/GE interface. To this end, this minireview focuses on the LM/GE interface by summarizing the main challenges comprehensively, recapitulating emerging strategies for these challenges, and providing perspectives for future research.

## 1. Introduction

With the explosive boom in the fields of portable electronics and electric vehicles, lithium-ion batteries (LIBs) have achieved remarkable success in the market. Conventional LIBs normally consist of carbon anodes, flammable organic electrolytes (OEs) and Li-containing oxides, challenging with unsatisfied energy density and poor safety. To further boost the energy density, lithium metal (LM) has been widely deemed as an ultimate anode candidate due to its highest theoretical specific capacity (3860 mAh/g, more than 10 times of the current commercial carbon anodes) and lowest electrochemical potential ( $-3.04$  V versus standard hydrogen electrode). However, the uncontrollable dendrite growth of LM during cycling can give rise to serious security risks, impeding its successful use in LIBs.<sup>[1]</sup> Replacing the OEs with solid-state electrolytes (SSEs) and naturally building all-solid-state Li metal batteries (ASSLMBs) are promising to completely address the fire and dendrite issues of LM-based batteries because SSEs possess non-flammability and high mechanical strength.<sup>[2]</sup> In this regard, ASSLMBs are on the cusp of being the most appealing next-generation energy storage systems.

Generally, SSEs used in ASSLMBs mainly belong to two groups: polymer electrolytes (PEs) and inorganic electrolytes

(IEs).<sup>[3]</sup> PEs are flexible and processable, and meanwhile hold good wetting ability toward electrodes. However, the development of PEs-based ASSLMBs has been limited by the poor room-temperature ion conductivity of PEs.<sup>[4]</sup> In contrast, IEs possess satisfactory ion conductivity, outstanding thermal stability as well as high Young's modulus. Among various IEs, garnet electrolytes (GEs) are being actively investigated owing to their high room-temperature ion conductivity ( $10^{-3}$  S/cm), excellent stability against LM and wide electrochemical potential window since Weppner's group originally reported the cubic phase  $\text{Li}_7\text{La}_3\text{Zr}_2\text{O}_{12}$  (LLZO).<sup>[5]</sup> Following this discovery, massive attempts to dope cations and optimize sintering process are motivated by concerns of fast ionic conduction.<sup>[6]</sup> Although the ion conductivities of GEs from these methods are comparable to OEs, the interfacial resistances are too large to enable GEs-based ASSLMBs competitive to commercial LIBs.<sup>[7]</sup> Moreover, fast short circuits of the GEs-based ASSLMBs can sometimes be induced by the daunting Li dendrite issue, which is closely related to the properties of LM/GE interface.<sup>[8]</sup> Therefore, the LM/GE interface plays vital roles in the electrochemical performance of GEs-based ASSLMBs. Understanding and improving the interface between LM and GE are of importance for enhancing the overall cell performance.

In this minireview, we firstly summary the main challenges of LM/GE interface, including large interfacial resistance and uncontrollable Li dendrite growth, followed by systematically discussing the recent advances in improving LM/GE interface. Among the various strategies, removal of  $\text{Li}_2\text{CO}_3$ , the introduction of alloy or soft interlayers, design of metal anodes, and changes of the physical and chemical properties of GEs are underscored (Figure 1). Finally, general conclusions of current limitations and perspectives for recommended future research directions are presented.

[a] J. Wang,<sup>+</sup> Prof. X.-B. Zhang  
State Key Laboratory of Rare Earth Resource Utilization  
Changchun Institute of Applied Chemistry  
Chinese Academy of Sciences  
Changchun, 130022, P. R. China  
E-mail: xzbzhang@ciac.ac.cn

[b] J. Wang<sup>+</sup>  
Key Laboratory of Automobile Materials, Ministry of Education,  
Department of Materials Science and Engineering  
Jilin University  
Changchun, 130022, P. R. China

[c] Dr. G. Huang<sup>+</sup>  
Materials Science and Engineering, Physical Science and Engineering Division  
King Abdullah University of Science and Technology (KAUST)  
Thuwal, 23955-6900, Saudi Arabia

[<sup>+</sup>] These authors contributed equally to this work.

 An invited contribution to a Special Collection on Lithium Metal Anode Processing and Interface Engineering

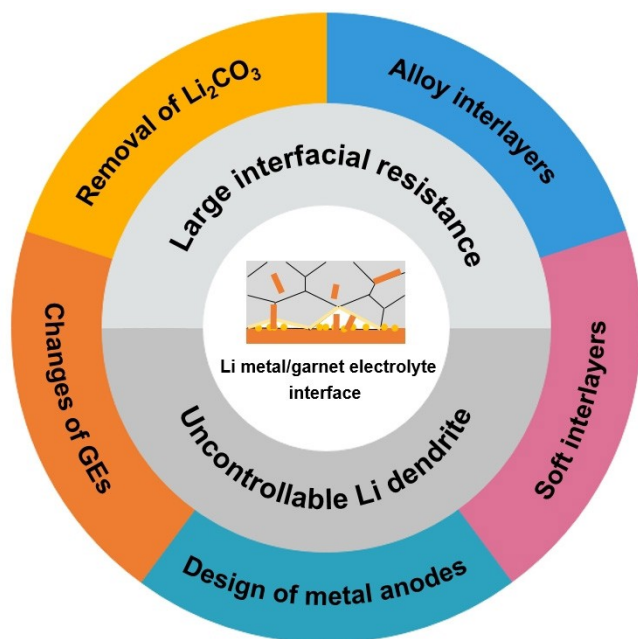


**Figure 1.** An overview of LM/GE interface, including its challenges and responding strategies.

## 2. Challenging Issues at the LM/GE Interface

### 2.1. Large Interfacial Resistance

High electrochemical/chemical stability is one of the reasons for the popularity of GEs. However, Han et al. revealed that the intrinsic electrochemical stability window of LLZO was 0.05–2.91 V (Figure 2a), which was smaller than the previously reported value of 0–6 V.<sup>[9]</sup> Moreover, first-principle calculation and experimental results confirmed that LLZO might be reduced into  $Zr_3O$ ,  $Li_2O$  and  $La_2O_3$  when contacting LM, while the  $Zr_3O$  could be further reduced into Zr metal. Most of these reduction products are poor ionic conductors, causing high

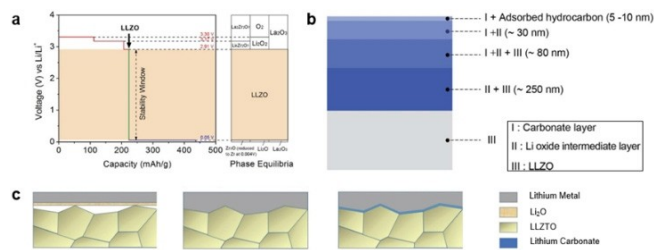


**Figure 2.** a) First principles calculation results of the voltage profile of LLZO upon lithiation and delithiation. Reproduced with permission from Ref. [9]. Copyright (2016) Wiley-VCH. b) Schematic of the contamination layers on the surface of LLZO. Compositions and thickness of each layer were detected by XPS analysis. Reproduced from Ref. [13]. Copyright (2016), with permission from Royal Society of Chemistry. c) Schematic of different wetting behaviors of LLZTO surfaces with molten LM. Reproduced from Ref. [11]. Copyright (2017), with permission from Wiley-VCH.

interfacial resistance. Zhu and co-workers also observed measurable LM induced reduction of  $Zr^{4+}$  in Ta/Nb/Al doped LLZO samples (denoted as LLZTO (or LLZT)/LLZNO/LALZO).<sup>[10]</sup> Besides the  $Zr^{4+}$ ,  $Nb^{5+}$  in LLZNO could also be significantly reduced. Therefore, the increasing interfacial resistance caused by GEs' limited electrochemical/chemical stability should be taken seriously.

Owing to the stiffness of GEs, heating has been widely adopted to achieve close contact between LM and GEs. Although first-principle calculation results indicate that the GE exhibit intrinsic lithiophilic property towards LM,<sup>[11]</sup> poor wetting behavior will still occur even after heating the LM/GE interface, arousing large interfacial resistance. With the aid of spectroscopy studies, Doeff' group revealed that  $Li_2CO_3$  contaminant was formed on the surface of GEs when they were exposed to air, which was regarded as the main origin of poor wettability towards LM.<sup>[12]</sup> After simply removing the  $Li_2CO_3$  by polishing, the wettability of the GEs surface was greatly enhanced, which further confirmed that  $Li_2CO_3$  was indeed the fundamental reason for the lithiophobic surfaces of GEs. A widely accepted reaction for the formation of  $Li_2CO_3$  was



Jin Wang received her B.S. degree in materials science and engineering from Changchun University of Science and Technology in 2015. She is currently pursuing a Ph.D. in materials science at Jilin University of China. Her current interests include design and synthesis of solid-state electrolytes for lithium-air batteries and Li metal protection.



Gang Huang received his PhD in applied chemistry from Changchun Institute of Applied Chemistry (CIAC) in 2016. Now he works at King Abdullah University of Science and Technology (KAUST) as a post-doctoral fellow and his research focuses on the development and characterization of nanoporous materials for Li-ion and Li-O<sub>2</sub> batteries.



Xin-Bo Zhang is a full professor at Changchun Institute of Applied Chemistry (CIAC), Chinese Academy of Sciences (CAS). He obtained his Ph.D. degree in inorganic chemistry from CIAC. His interests mainly focus on functional inorganic materials for batteries, fuel cells, and electrochemical catalysis.

proposed by Sakamoto' group with the combination of experimental measurements and computational modeling.<sup>[13]</sup> Figure 2b illustrates the distribution of contaminant layers on the surface of LLZO. Firstly, LiOH forms through  $\text{Li}^+/\text{H}^+$  exchange between LLZO and moisture. Carbonation of LiOH is subsequently happened, generating  $\text{Li}_2\text{CO}_3$  contaminant. Moreover, the amount of  $\text{Li}_2\text{CO}_3$  strongly depends on the exposure time and relative humidity (RH) level. With the increase of exposure time and RH, the amount of  $\text{Li}_2\text{CO}_3$  significantly increases. In a later study, Xia et al. identified  $\text{LiOH}\cdot\text{H}_2\text{O}$  as a necessary intermediate to form  $\text{Li}_2\text{CO}_3$ .<sup>[14]</sup> Although the mechanism for  $\text{Li}_2\text{CO}_3$  formation is still far from well clarified at the moment, it is necessary to control the influencing factors for reducing its formation. Jin et al. and Brugge et al. observed that  $\text{Li}_2\text{CO}_3$  preferred to grow in grain boundaries through scanning electron microscope (SEM) and impedance analysis, respectively.<sup>[15]</sup> Similarly, Xia et al. reported that GEs sintered in Pt crucible possessed better air stability and lower interfacial resistance than that sintered in  $\text{Al}_2\text{O}_3$  crucible, because the former GE had fewer grain boundaries than the latter one, which was consistent with the prevailing understandings.

Inversely, Zheng et al. believed that it was not the contaminants on the LLZTO surface, but the oxide layer on the LM that largely determined the interfacial wettability.<sup>[11]</sup> As depicted in Figure 2c, regardless of the presence or absence of  $\text{Li}_2\text{CO}_3$  on the surface of the LLZTO, LLZTO could be wetted well by clean LM. First-principle calculation results demonstrated that the interface formation energy of  $\text{Li}_2\text{CO}_3/\text{Li}$  and  $\text{Li}_2\text{O}/\text{Li}$  are  $-0.63$  and  $0.23$  J/m<sup>2</sup>, respectively. This clearly indicates that  $\text{Li}_2\text{CO}_3$  facilitates wetting to some extent, while  $\text{Li}_2\text{O}$  absolutely impedes it. Evidently,  $\text{Li}_2\text{O}$  on the surface of LM plays a more dominant role than the surface  $\text{Li}_2\text{CO}_3$  layer of LLZTO in terms of wetting LM. The interfacial area specific resistance (ASR) of clean Li/LLZTO was  $6.95$   $\Omega/\text{cm}^2$ , much smaller than the thousands of ohms ever reported.<sup>[12,16]</sup>

## 2.2. Uncontrollable Li Dendrite

Newman et al. held a view that the Li dendrite could be eliminated when the shear modulus of electrolyte was more than twice that of LM (3.4 GPa).<sup>[17]</sup> But this guideline only works to LM/PE interface, not to LM/GE interface. Numerous reports have observed that Li dendrite forms easily and penetrates GE fast even if the shear modulus of GEs is about 60 GPa.<sup>[18]</sup> In order to accurately describe the ability of SSEs in terms of suppressing Li dendrite growth, a concept of "critical current density (CCD)" has been proposed, which stands for maximum current density that SSEs can withstand before short circuit. To date, the CCD of the GEs is only around  $0.5$  mA/cm<sup>2</sup>, far from the goal of  $3\text{--}10$  mA/cm<sup>2</sup>.<sup>[3]</sup>

The poor contact between LM and GE makes  $\text{Li}^+$  ions concentrate at the confined contact points of the Li/GE interface (Figure 3a), resulting in inhomogeneous distribution of  $\text{Li}^+$  ions. Consequently, dendrite forms at these "hot spots".<sup>[19]</sup> In addition, Li stripping may produce new voids at the LM surface if the dissolved Li cannot be replenished in

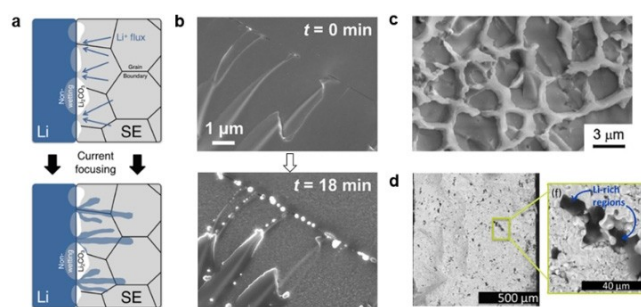


**Figure 3.** a) Potential microstructural contributions to inhomogeneous Li deposition with concentrated  $\text{Li}^+$ . Reproduced with permission from Ref. [19c]. Copyright (2018) American Chemical Society. b) SEM images during Li deposition on LLZTO cross-section with a current density of about  $200$  mA/cm<sup>2</sup> using electron beam. Preferred nucleation sites along cracks and ledges can be seen. Reproduced from Ref. [23]. Copyright (2019), with permission from Elsevier. c) SEM image of the web-structure LM deposition along the grain boundaries in cycled GE. Reproduced from Ref. [27]. Copyright (2017), with permission from Elsevier. d) SEM image of the cycled GE. Reproduced with permission from Ref. [31b]. Copyright (2017) American Chemical Society.

time. These new voids will further deteriorate the interface contact and accelerate the Li dendrite growth. Recently, Wang et al. proposed a new terminology named critical stack pressure to define the balance point where incoming Li flux from the applied stack pressure is equal to dissolving Li.<sup>[20]</sup> Since the rate of Li replenishment is proportional to the adatom diffusion rate of LM and the applied stack pressure can facilitate adatom diffusion, it is obvious that the applied stack pressure should be higher than the critical stack pressure to avoid new voids formation, as a result, increasing the CCD to some extent.<sup>[20–21]</sup> Besides, power-law creep model and experimental results presented that the Li adatom diffusion rate could be significantly improved even with a slight increase of temperature.<sup>[22]</sup> What's more, Krauskopf et al. revealed the Li adatom diffusion rate in Li–Mg alloy was much faster than in LM.<sup>[22b]</sup> Therefore, enlarging pressure and increasing temperature, as well as using alloys are all instructive for maintaining intimate LM/GE interface contact and alleviating "hot spots".

In addition to these "hot spots", morphological flaws, such as cracks and ledges, on the GEs surface are also the suspicious location for Li dendrite formation (Figure 3b).<sup>[23]</sup> Many groups have observed that whisker/sphere/cluster/filament-like Li dendrite preferentially deposits on the surface flaws of the GEs through in operando optical microscope.<sup>[23–24]</sup> Under the stress generated by dendrite penetration, new cracks appeared beside the pre-existed ones. Using a continuum model, Bucci et al. concluded that a driving force generated by stress increased with the increase of crack length.<sup>[25]</sup> Hence, crack and stress promoted each other until the crack penetrated across the GEs, resulting in short circuit.

Grain boundary is another pathway for Li dendrite growth.<sup>[26]</sup> Sakamoto et al. directly observed that the Li dendrite propagated intergranularly through the grain boundaries of GEs by SEM (Figure 3c).<sup>[27]</sup> Molecular dynamics simulations revealed that shear modulus at grain boundaries was 50% lower than that at bulk regions.<sup>[19c]</sup> This remarkable softening in

elastic properties is considered as the primary origin for Li deposition near grain boundaries. Inhomogeneous ionic conductivities between grain boundary and bulk region appear to be another possible reason.<sup>[28]</sup> It is generally believed that the differences of composition at grain boundaries and grains cause inhomogeneous ionic conductivities.<sup>[29]</sup> But Smetacek et al. claimed that neither local Al content nor local Li content had an obvious correlation with the local ionic conductivity in LLZO.<sup>[30]</sup> Maybe other factors have pronounced effects on the difference in ionic conductivity, which requires further study.

Instead of propagating from one electrode to another, isolated Li dendrite within GE has been observed frequently (Figure 3d).<sup>[31]</sup> Density functional theory (DFT) calculations demonstrated that  $e^-$  was thermodynamically favorable to be trapped by La atom in GE, which might cause LM to deposit directly inside the GE.<sup>[32]</sup> Consistently, Janek's group presented fast Li nucleation inside the LLZO after  $e^-$  injection.<sup>[23]</sup> By comparing the growth behaviors of Li dendrite in LLZO, LiPON and  $\text{Li}_3\text{PS}_4$ , Han et al. found that the CCDs of electrolytes were proportional to their electronic conductivities. Evidently, the relatively high electronic conductivity of GE is strongly responsible for the fast Li dendrite growth inside GE.

### 3. Strategies for Improving the LM/GE Interface

#### 3.1. Removal of $\text{Li}_2\text{CO}_3$

Considering that the formation of  $\text{Li}_2\text{CO}_3$  is almost inevitable during the storage of GEs, removal of the formed  $\text{Li}_2\text{CO}_3$  is a practical solution for improving the LM/GE interface. Typical mechanical polishing has become a widely accepted pre-treatment method,<sup>[1,2,33]</sup> but it is insufficient to completely remove  $\text{Li}_2\text{CO}_3$ , meanwhile more flaws will be introduced on the electrolyte surface after polishing. Through reacting LLZO with carbon (LLZO-C) at 700 °C (Figure 4a), Li et al. successfully removed  $\text{Li}_2\text{CO}_3$  and lowered the interfacial ASR to 28  $\Omega/\text{cm}^2$ .<sup>[34]</sup> In a later work, Cheng et al. claimed that the  $\text{Li}_2\text{CO}_3$ -contaminated GEs could be recovered after heating at 250 °C under inert atmosphere.<sup>[35]</sup> These conventional thermal treatments are generally time-consuming, and potential to generate impurity phase due to the high-temperature induced Li loss. Reducing the thermal treatment temperature is the future development direction in this field. For avoiding thermal treatment, Sun'

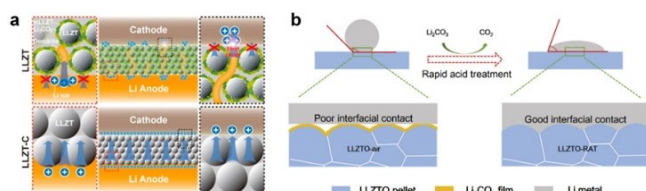


**Figure 4.** a) Schematic of ASSEMBs with LLZT and LLZT-C. Reproduced with permission from Ref. [34]. Copyright (2018) American Chemical Society. b) Schematic illustration of Li/LLZTO interface before and after the rapid acid treatment. Reproduced from Ref. [36]. Copyright (2019), with permission from Elsevier.

group proposed rapid HCl treatment to remove the surface  $\text{Li}_2\text{CO}_3$  of LLZO within one minute (Figure 4b).<sup>[36]</sup> This method could also be extended to other acids, such as  $\text{H}_2\text{SO}_4$  and  $\text{H}_3\text{PO}_4$ . Interestingly,  $\text{H}_3\text{PO}_4$  can not only remove contaminants, but also generate  $\text{Li}_3\text{PO}_4$  layer.<sup>[37]</sup> This  $\text{Li}_3\text{PO}_4$  layer converts the surface of GE from lithiophobic to lithiophilic, leading to a dramatically reduced interfacial ASR of 7  $\Omega/\text{cm}^2$ . Moreover,  $\text{Li}_3\text{PO}_4$  is capable of inhibiting Li dendrite penetration, boosting the battery performance significantly. Although acid treatment is facile and fast, it is still hard to remove all the  $\text{Li}_2\text{CO}_3$ , especially the one inside the GEs. Thus, it is most important to increase the intrinsic air stability of GEs.

#### 3.2. Alloy Interlayers

Considering that the surface chemical components of GEs strongly affect the wettability to LM and  $\text{Li}^+$  distribution, it is effective to introduce an interlayer between GE and LM, which has strong chemical binding energy with LM to ameliorate the LM/GE interface. Specifically, Han and co-workers successfully introduced a 5 nm coating of  $\text{Al}_2\text{O}_3$  on the GE by atomic layer deposition (ALD).<sup>[38]</sup> This vapor deposition method ensures the rugged GE surface to be completely covered by  $\text{Al}_2\text{O}_3$ . The subsequently heating induced formation of Li–Al alloy interface makes LM well wet GE along with significant decrease of interfacial ASR to 1  $\Omega/\text{cm}^2$  (Figure 5a–5b). After this, numerous materials that could be alloyed with LM have been employed to wet the GE, such as Si,<sup>[39]</sup> Mg,<sup>[40]</sup> Ge,<sup>[41]</sup> ZnO,<sup>[42]</sup> Ag,<sup>[43]</sup> and InO,<sup>[44]</sup> and most of these interlayers have been prepared through the techniques like plasma-enhanced chemical vapor deposition (PECVD), ALD, magnetron sputtering (MS) and thermal evaporation (TE). Note that these methods are

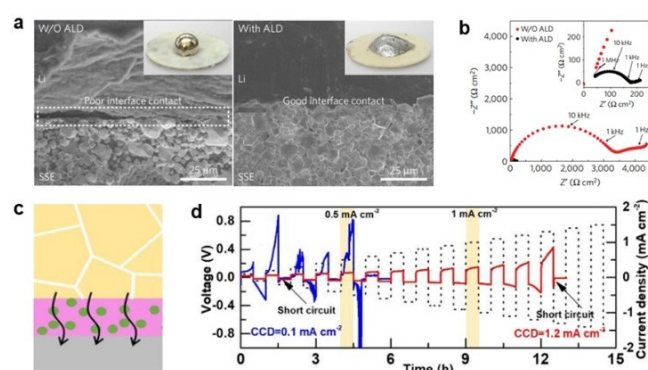


**Figure 5.** a) SEM images of the GE/LM interface. Without ALD- $\text{Al}_2\text{O}_3$  coating, GE has poor contact with LM even after heating. With the help of ALD- $\text{Al}_2\text{O}_3$  coating on GE, LM can uniformly bond with GE at the interface after heating. Inset are photos of melted LM on the surface of the GE, demonstrating classical wetting behavior for ALD-treated GE surface. b) Comparison of EIS curves of the symmetric Li/Li cells with GEs. Inset shows the enlarged impedance curves of the ALD-treated GE cell. (a) and (b) are reproduced from Ref. [38]. Copyright (2016), with permission from Springer Nature. c) Schematic of electric field distribution in MCL. Red, green, yellow and gray areas represent  $\text{Li}_3\text{N}$  matrix, Cu nanoparticle, GE and LM, respectively. d) CCD of the symmetric Li/Li batteries with GE (blue curve) and the GE protected by MCL (red curve). (c) and (d) are reproduced from Ref. [33]. Copyright (2008), with permission from Royal Society of Chemistry.

relatively complicated, simple and easy strategies are still needed.<sup>[45]</sup> What's more, recent works showed that the alloy interlayers underwent huge volume change during repeated alloying/dealloying processes, accompanied with the loss of intimate contact between LM and GE, leading to the deterioration of battery performance.<sup>[46]</sup> In response, Feng et al. reported a  $\text{Cu}_6\text{Sn}_5$  alloy interlayer with limited Sn diffusion and stable framework that could effectively mitigate the volume change for maintaining a good interface contact.<sup>[47]</sup>

Recently, adding ion conductors into alloy interlayers has been investigated to enable superior battery performance.<sup>[33]</sup> A new study from Sun's group designed a mixed conductive layer (MCL) by embedding electronic conductive Cu nanoparticles into  $\text{Li}_3\text{N}$  ionic conductive network through reacting the  $\text{Cu}_3\text{N}$  film with molten LM.<sup>[33]</sup> The Cu nanoparticles provide homogeneous electronic field, while the  $\text{Li}_3\text{N}$  matrix ensures fast  $\text{Li}^+$ -conducting pathways (Figure 5c). Benefiting from this synergy effect, the interfacial ASR reduced from  $1138.5 \text{ } \Omega/\text{cm}^2$  to  $83.4 \text{ } \Omega/\text{cm}^2$ , and the CCD increased from  $0.1 \text{ mA}/\text{cm}^2$  to  $1.2 \text{ mA}/\text{cm}^2$  (Figure 5d). The CCD of GE with this MCL is higher than that of most GEs modified with pure alloy interlayers. Similarly, mixtures of alloys and  $\text{Li}_2\text{O}$ ,<sup>[48]</sup>  $\text{LiF}$ <sup>[49]</sup> or  $\text{LiNbO}_3$ <sup>[50]</sup> have also played a positive role in reducing the interfacial ASR and increasing the CCD. However, using  $\text{Li}_3\text{N}$  alone as the interlayer gave rise to large interfacial ASR exceeding  $160 \text{ } \Omega/\text{cm}^2$  even at  $60^\circ\text{C}$ , highlighting the importance of synergy effect of ion conductors and electron conductors.<sup>[51]</sup>

There are many factors from alloy interlayers having pronounced effects on the battery performance, among which the composition of the alloy interlayers is a decisive factor towards interface properties.<sup>[52]</sup> Very recently, Kim et al. observed different morphologies of Li deposition on the GEs modified with Si/Au/Ag layer.<sup>[24c]</sup> LM preferentially deposited at only a few sites and grew into whisker-shaped dendrite on Si layer. Although Au layer guided Li to precipitate with island-like shape, it failed to achieve uniform deposition. In sharp contrast, the Ag layer achieved a uniform Li deposition by providing numerous small nuclei. These distinguishing deposition behaviors might originate from the different solubilities of various metals in LM. The greater the solubility, the lower the energy barrier is required for LM nucleation and thus uniform LM deposition. In other words, the alloy interlayer is not only a buffer layer for Li redistribution, but also a matrix for facile Li precipitation.

Apart from the composition of the interlayers, the speed of  $\text{Li}^+$  transfer in the interlayer matrix, which strongly related to the crystallinity of the interlayers, is also an important factor towards interface properties. Unlike previous highly graphitized carbon (HGC) interlayers, low graphitized carbon (LGC) with amorphous structure was recently reported to serve as an interlayer by Feng et al.<sup>[53]</sup> For HGC,  $\text{Li}^+$  could only transfer horizontally, while the disordered structure of LGC provided many more  $\text{Li}^+$  transfer pathways, resulting in faster lithiation speed of LGC than that of HGC. Besides,  $\text{Li}_2\text{CO}_3$  contaminant disappeared by carbothermal reduction ( $\text{Li}_2\text{CO}_3 + \text{C} \rightarrow \text{Li}_2\text{O} + 2\text{CO}$ ) during the synthesis of LGC through thermal-decomposition vapor deposition (TVD) method. Consequently, a low

interfacial ASR of  $9 \text{ } \Omega/\text{cm}^2$  and high CCD of  $1.2 \text{ mA}/\text{cm}^2$  were achieved, which were the best results among the reported works with Li-C alloy interlayers.

The physical properties of the alloy interlayers, such as thickness and hardness, also need to be taken seriously in fundamental research. As investigated by Chen et al., Si interlayer failed to maintain intimate contact with GE unless the thickness was small than  $180 \text{ nm}$ .<sup>[54]</sup> As the thickness increased, the battery performance continuously deteriorated, and only a few cycles could be delivered when the thickness of Si layer close to  $900 \text{ nm}$ .

The above alloy interlayers can undoubtedly improve the interface contact and suppress the dendrite growth to some extent, but it is unfortunate that short circuit will still happen if the current density exceeds the CCD. To conquer this, Fu and co-workers proposed an intelligent interlayer to avoid short circuit by taking advantage of the conversion reaction between  $\text{MoS}_2$  and Li.<sup>[55]</sup> The concentrated current density near Li dendrite promoted the reaction between  $\text{MoS}_2$  and Li dendrite to generate  $\text{Li}_2\text{S}/\text{Mo}$  layer with characterizations of poor electronic and  $\text{Li}^+$  conductivity, thereby suppressing the further growth of Li dendrite. Instead of short circuit, obvious polarization up to  $5 \text{ V}$  occurred when the current density increased to  $2.2 \text{ mA}/\text{cm}^2$ .

From the above examples, it is obvious that the alloy interlayers can facilitate close contact with the GEs, thereby achieving low ASR. However, the severe volume expansion of the alloy interlayers during battery operation will rapidly deteriorate the interfacial contact, limiting the lifetime of the battery. Fine adjustments of the physical and chemical properties of the alloy interlayers are expected to alleviate this problem.

### 3.3. Soft Interlayers

Adding a minimal amount of OEs or gel polymer electrolytes (GPEs) between GE and LM can easily improve the interfacial contact.<sup>[56]</sup> With a soft and bendable PVDF-HFP-based GPE interlayer, Liu et al. successfully decreased the interfacial ASR from  $1.4 \times 10^3$  to  $214 \text{ } \Omega/\text{cm}^2$ .<sup>[56a]</sup> It should be noted that the absorbed OEs in GPEs still have security risks. Moreover, Bruce' group found LP30 ( $\text{LiPF}_6$  in ethylene carbonate and dimethyl carbonate), a kind of commercial OE, was unstable with LLZTO and a  $\text{Li}^+$ -conducting solid electrolyte interlayer composed of  $\text{LiF}$ ,  $\text{Li}_2\text{O}$ ,  $\text{Li}_2\text{CO}_3$  and organic compositions was detected on the surface of LLZTO (Figure 6a).<sup>[57]</sup> This made the interfacial ASR increase with time and finally stabilize at around  $580 \text{ } \Omega/\text{cm}^2$  (Figure 6b), which was much higher than the combined resistance of LLZTO itself and Li/LLZTO interface. Accordingly, stabilizing the OE/LLZTO interface is a primary prerequisite when adopting OEs or GPEs as interlayers. By adding *n*-BuLi, the interfacial ASR of OE/GE interface almost kept constant during cycling in  $\text{LiFePO}_4/\text{Li}$  battery, because *n*-BuLi could not only suppress  $\text{Li}^+/\text{H}^+$  exchange, but also retard the formation of resistive interlayer derived from by-reactions (Figure 6c).<sup>[58]</sup> Up to now, the evolutions of interfaces between various OEs

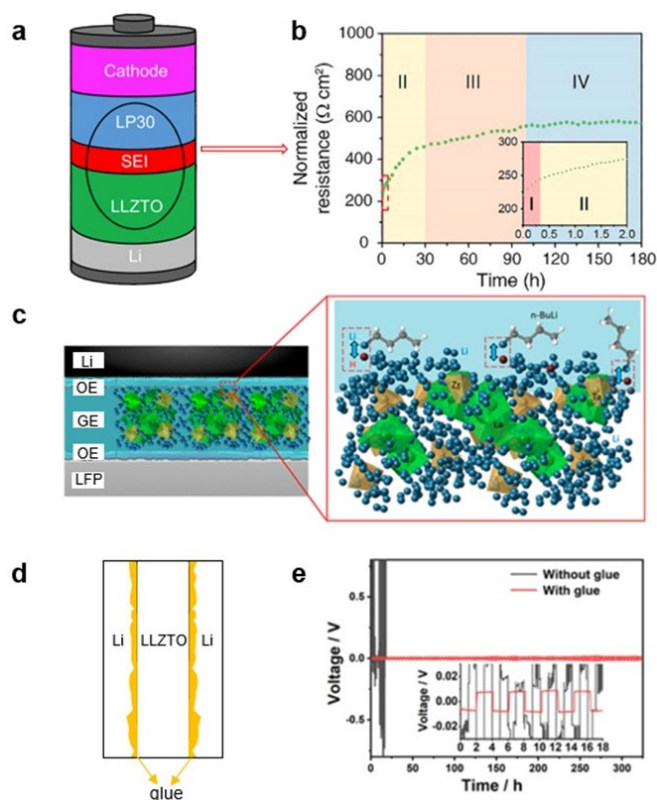


**Figure 6.** a) Schematic of battery contains LLZTO/LP30 interface. b) Interfacial ASR of the LLZTO/LP30 interface with time. According to different trends, the time dependence is categorized into four regions, I, II, III, and IV. (a) and (b) are reproduced from Ref. [57]. Copyright (2020) Elsevier. c) Illustration of the effect of *n*-BuLi on stabilizing the OE/GE interface. Reproduced with permission from Ref. [58]. Copyright (2017) American Chemical Society. d) Schematic diagram of LLZTO-based symmetric Li/Li battery with glue interlayer. e) Voltage profiles of the LLZTO-based symmetric Li/Li battery with and without glue interlayer (current densities: 0.05 mA/cm<sup>2</sup>). (d) and (e) are reproduced with permission from Ref. [61]. Copyright (2017) American Chemical Society.

and GEs are unclear and detailed researches are urgently needed. In addition, the interface stabilizers like *n*-BuLi deserve more attention.

PEs with excellent flexibility and relatively high safety have also been used as interlayers. For example, Duan et al. modified the GE surface with an ultrathin PEGMEA-based PE.<sup>[59]</sup> Symmetric Li/Li battery with this modified GE delivered flat and stable voltage plateau for over 3200 h at a current density of 0.1 mA/cm<sup>2</sup> without discerned Li dendrite formation. Unfortunately, most GEs-based batteries with PEs interlayers have to operate above 50 °C due to the unsatisfactory room-temperature ionic conductivity and poor adhesive ability of PEs.<sup>[60]</sup> Recently, Dong et al. developed a PIN@SN polymer glue, which was liquid at room temperature and could be solidified after “post curing stage”, to behave as conformal caulking agent for LM/LLZTO interface (Figure 6d).<sup>[61]</sup> Meanwhile, this polymer glue exhibited high peel-off strength (70–90 N/cm) and good ionic conductivity at room temperature (1.15 × 10<sup>-4</sup> S/cm). Given these advantages, the interfacial ASR of LM/LLZTO interface reduced from 5114 to 104 Ω/cm<sup>2</sup> and the symmetric Li/Li battery cycled stably for up to 300 h at room temperature (Figure 6e).

Generally, the PEs not only show lower ionic conductivities than that of the GEs, but also possess narrower electrochemical stability windows. This will undoubtedly sacrifice the advantages of the GEs-based ASSLMBs. In consideration of this dilemma, composite solid electrolytes which combine the merits of PEs and GEs are regarded as strong candidates.

In order to intuitively compare the strategies used for preparing the interlayers in sections 3.2 and 3.3, their advantages and disadvantages are listed in Table 1. It is clear that each technique more or less has some problems. More works should be done to conquer these to further improve the battery performance or make the technique with application prospect.

### 3.4. Design of Metal Anodes

Generally, alloying elements are normally added to adjust the viscosity and surface energy of the liquid metals to decrease the contact angle with ceramic substrates in the field of brazing. Instead of LM, molten Li–Sn alloy,<sup>[62]</sup> Li–Al alloy<sup>[63]</sup> and Li–C alloy<sup>[64]</sup> all exhibited reduced contact angles (<90°) toward GEs without compromised ductility. These Li alloy/GE/Li alloy cells delivered interfacial ASR as low as 1 Ω/cm<sup>2</sup> and endured a high CCD up to 1 mA/cm<sup>2</sup>. Interestingly, although the alloys experienced significant volume changes, the interfaces between GEs and alloys were more stable than that with LMs. Notably, Hu’s group and Janek’s group all claimed that Li–Mg alloy could effectively alleviate contact loss with GEs.<sup>[22b,65]</sup> The Li–Mg alloy served as an ion/electron dual-conductive Li host and cycled as a Li-rich and Li-deficient alloy during Li plating and stripping, respectively. This alloy framework kept seamless interface contact with GE even after stripping a large amount of Li without generating gaps or voids. Combining Li alloys and inorganic Li<sup>+</sup> conductors as anodes in ASSLMBs can further increase the CCD. In a recent study, Huang’s group prepared Li<sub>3</sub>N added Li–C alloy through heating molten LM and g-C<sub>3</sub>N<sub>4</sub> at 280 °C (Figure 7a).<sup>[66]</sup> Although the interfacial ASR of the symmetric cell with Li<sub>3</sub>N added Li–C alloy or Li–C alloy electrode was the same (11 Ω/cm<sup>2</sup>), the CCD of Li<sub>3</sub>N added Li–C alloy based symmetric cell (1.5 mA/cm<sup>2</sup>) was

Table 1. Summary of the strategies for preparing the interlayers.			
Strategy	Technique	Advantages	Disadvantages
Deposition	MS, ALD, TVD, PECVD	Precise controllability and large-scale production	Complicated
Wet chemical	Reduction of metal ions	Cheap and fast	Unmanageable and easy to produce by-products
Physical method	Mechanical grinding and spraying	Facile manufacturing	Generate uneven and poor connection between interlayer and GE
Others	In situ polymerization, blade casting and spinning	Good processability	Cumbersome

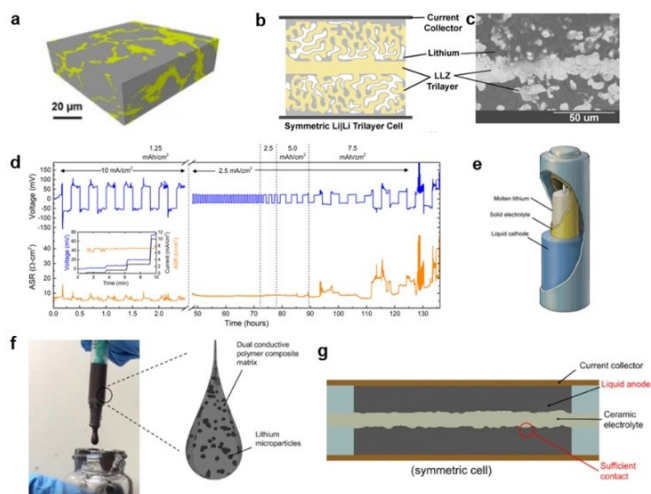


**Figure 7.** a) 3D rendering image of the  $\text{Li}_3\text{N}$  added Li–C alloy. Yellow and gray areas represent LM and reacted  $\text{g-C}_3\text{N}_x$ , respectively. Reproduced from Ref. [66]. Copyright (2020), with permission from Wiley-VCH. b) Diagram of trilayer symmetric Li/Li battery. c) SEM image of trilayer GE with two porous layers filled with LM. d) Voltage profiles (blue) and interfacial ASR (orange) response of trilayer symmetric Li/Li battery during battery operation. (b), (c), and (d) are reproduced from Ref. [67a]. Copyright (2019), with permission from Elsevier. e) Schematic of battery contains liquid LM/GE interface. Reproduced from Ref. [68b]. Copyright (2018), with permission from Springer Nature. f) Digital picture and schematic diagram of SLMA. g) Schematic illustration of symmetric SLMA/SLMA cell with GE. (f) and (g) are reproduced from Ref. [70]. Copyright (2019), with permission from Elsevier.

much higher than that of Li–C alloy based symmetric cell ( $1 \text{ mA/cm}^2$ ).<sup>[64,66]</sup> It is obvious that the alloy anodes have advantages in wetting the interface of GEs and keeping the interface stable. Unluckily, the use of alloy anodes does reduce the energy density to some extent. Therefore, a balance needs to be achieved between high energy density and good interfacial contact.

The conventional 2D plane contact between LM and GE is challenging with limited contact area and contact loss caused by volume change. Turning from 2D contact to 3D contact has been confirmed to be effective in alleviating these problems.<sup>[67]</sup> By means of tape casting, a GE skeleton with porous-dense-porous trilayer structure was developed by Wachsman et al.<sup>[67a]</sup> The porous layers acted as electrode supports and enlarged the interfacial surface area by more than forty times than the conventional 2D plane interface. Symmetric cell with LM filled into the pores of the porous layer successfully cycled up to  $10 \text{ mA/cm}^2$  with interfacial ASR of  $2\text{--}10 \text{ }\Omega/\text{cm}^2$  (Figure 7b–7d). Meanwhile, the large volume changes of LM could be accommodated by the porous skeleton of GE. It should be warned that although symmetric cell with this 3D electrode can operate normally at high current density, this is just due to the increased surface area. The CCD per unit area is not greatly improved.

Besides, operating batteries above the melting point of LM is another way to decrease the interfacial resistance. Cui and co-workers conducted in-depth studies on the liquid LM/GE interface (Figure 7e).<sup>[68]</sup> In their studies, the ion conductivity of GE remarkably enhanced and the ASR of liquid LM/GE interface

was smaller than  $0.4 \text{ }\Omega/\text{cm}^2$ . However, the high temperature for keeping LM in liquid state is energy-consuming and corrosive. In a later research, Li et al. demonstrated a semiliquid LM anode (SLMA) by dispersing in situ generated Li microparticles in electron/ion dual-conductive liquid polymer composite (Figure 7f).<sup>[69]</sup> This SLMA kept liquid throughout a wide temperature range from  $25^\circ\text{C}$  to  $150^\circ\text{C}$  and facilitated large-scale preparation. Owing to the intimate and conformal interfacial contact (Figure 7g), GE-based symmetric cell with the SLMA achieved stable voltage profile with overpotential about  $150 \text{ mV}$  at a current density of  $1 \text{ mA/cm}^2$  with 1 h half cycle time for nearly 400 h. However, the SLMA-based cell was cycled above room temperature ( $50^\circ\text{C}$ ) probably due to the slow  $\text{Li}^+$  transfer of the SLMA. Changing the PEO-based ion-conductive polymer to another one with superior  $\text{Li}^+$  transfer ability at room temperature may conquer this issue.

### 3.5. Changes of GEs

According to previous works, the physical and chemical properties of the GEs themselves deeply influence the characteristics of the LM/GE interface, so changing the GEs is promising to improve the interface. Adjusting the doping elements,<sup>[29a,71]</sup> downsizing to ultrafine powders,<sup>[72]</sup> optimizing the sintering process,<sup>[73]</sup> adding sintering aids,<sup>[29b,74]</sup> and applying advanced sintering technologies<sup>[75]</sup> are favorable methods to enhance the chemical/electrochemical stabilities of GEs and reduce  $\text{Li}_2\text{CO}_3$  impurity. For example, the introduction of just 2 wt.% hydrophobic LiF into LLZT (LLZT-2LiF) could effectively suppress  $\text{Li}_2\text{CO}_3$  formation in air (Figure 8a), demonstrating a significant decrease of interfacial ASR from  $1260$  to  $35 \text{ }\Omega/\text{cm}^2$  (Figure 8b).<sup>[76]</sup> Unfortunately, the LiF additive not only reduced the density but also worsened the ionic conductivity of LLZT. Guo's group put forward another interesting strategy by creating a Li-deficient shield on the surface of GE after calcinated it at  $900^\circ\text{C}$ .<sup>[77]</sup> This Li-deficient shield was capable of restraining the formation of  $\text{Li}_2\text{CO}_3$ , and thus  $\text{Li}_2\text{CO}_3$ -free GE could be obtained after removing the shield. As a result, a low interfacial ASR of  $49 \text{ }\Omega/\text{cm}^2$  was achieved. Although these methods successfully suppress the formation of  $\text{Li}_2\text{CO}_3$ , the ionic conductivities of the GEs all decrease, which will limit the  $\text{Li}^+$  transfer at high rate operation.

Besides, reducing the electronic conductivities of the GEs is also an effective approach to improve the CCD. Song et al. coated the  $\text{Li}_7\text{La}_{2.75}\text{Ca}_{0.25}\text{Zr}_{1.75}\text{Nb}_{0.25}\text{O}_{12}$  (LLCZN) powder with low-electronic-conductivity  $\text{LiAlO}_2$  by a simple chemical coating process (Figure 8c).<sup>[31a]</sup> The electronic conductivity of the  $\text{LiAlO}_2$  coated LLCZN ( $1.01 \times 10^{-8} \text{ S/cm}$ ) was almost three times lower than that of LLCZN without  $\text{LiAlO}_2$  layer ( $3.59 \times 10^{-8} \text{ S/cm}$ ), which significantly slowed the Li dendrite growth. Moreover, the  $\text{LiAlO}_2$  coated LLCZN exhibited much lower interfacial ASR and higher CCD ( $25 \text{ }\Omega/\text{cm}^2$ ;  $0.75 \text{ mA/cm}^2$ ) compared with those of pure LLCZN ( $4100 \text{ }\Omega/\text{cm}^2$ ;  $0.4 \text{ mA/cm}^2$ ). This method improves the CCD just by reducing the electronic conductivities of the grain boundaries. If the electronic conductivities of the

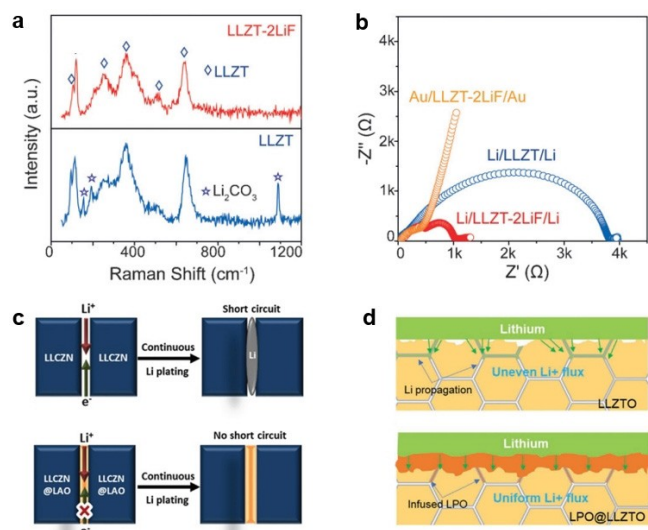


**Figure 8.** a) Raman spectra of LLZT and LLZT-2LiF after exposed to air for two weeks. b) EIS spectra of LLZT-2LiF and LLZT with Li electrodes. (a) and (b) are reproduced from Ref. [76]. Copyright (2016), with permission from Wiley-VCH. c) Schematic illustrations of Li dendrite formation within LLCZN and principle of suppressing it by means of surface coating. Reproduced from Ref. [31a]. Copyright (2019), with permission from Wiley-VCH. d) Schematic of Li dendrite suppression by coating and infusing GE with Li<sub>3</sub>PO<sub>4</sub>. Reproduced from Ref. [79]. Copyright (2020), with permission from Wiley-VCH.

grains can be reduced at the same time, a greater breakthrough is expected.

As important as avoiding the formation of Li dendrite, delaying the propagation of the Li dendrite that has already formed is also an effective strategy to prolong the battery life. As illustrated in Figure 8d, Xu et al. engineered the grain boundaries of LLZT by introduction of Li<sub>3</sub>PO<sub>4</sub> as a self-limiting sintering aid.<sup>[78]</sup> The Li<sub>3</sub>PO<sub>4</sub> additive was sufficient to prevent Li dendrite from propagating the LLZT, because Li<sub>3</sub>PO<sub>4</sub> was capable of in situ reacting with Li dendrite formed at grain boundaries. Most recently, Zhang's group coated and infused GE with Li<sub>3</sub>PO<sub>4</sub> through ALD and subsequent heating treatment.<sup>[79]</sup> This coated and infused Li<sub>3</sub>PO<sub>4</sub> was Li<sup>+</sup>-conductive but e<sup>-</sup>-insulating, which effectively suppressed the growth of Li dendrites and the direct reduction of the GE by LM, achieving a low ASR of 1 Ω/cm<sup>2</sup> and a high CCD of 2.2 mA/cm<sup>2</sup>. So, modifying the grain boundaries of GE and the interface between LM and GE at the same time is hopeful to achieve a long-lasting stabilization effect.

#### 4. Summary and Outlook

The attractive properties of GEs, such as high ion conductivity, excellent stability against LM as well as wide electrochemical potential window, make them one of the most promising candidates for ASSLMBs. After decades of development, significant progress has been achieved in GEs-based ASSLMBs. However, as the GEs-based ASSLMBs are still in infancy, the current GEs-based ASSLMBs are always faced with various

challenges, including but not limited to unsatisfactory LM/GE interface. In this minireview, we discussed the existing two main problems of the LM/GE interface and summarized the corresponding solutions (Table 2). Moreover, on this basis, some perspectives are proposed as follows:

- 1) Since the challenges of LM/GE interface and their origins are often interrelated, most of the existing approaches, which focus only on one of the problems of LM/GE interface, are far from achieving a favorable LM/GE interface. A comprehensive solution that can bring unexpected performance improvements is in crying need. In addition, it will be more instructive to study the LM/GE interface in a full cell than in a symmetrical cell.
- 2) Current research results have proved that the death of ASSLMBs is closely related to the interface failure during battery operation. Although researchers have conducted detailed studies on the LM/GE interfaces of freshly assembled ASSLMBs, the evolution of the interfaces during charging and discharging is still unclear. In addition, the LM/GE interface evolution in ASSLMBs is undoubtedly different when matched with various cathode materials (Li-contained oxides, sulfur, and O<sub>2</sub> etc.) Therefore, in operando and in situ characterizations with suitable battery models should be developed for getting precise information during battery operation.
- 3) Despite there are many solutions that can effectively reduce the interfacial ASR and increase the CCD, the detailed mechanism cannot be clearly unveiled based on experimental data alone. Simulation methods are essential for under-

**Table 2.** Summary of the ASR and CCD values of recently reported works.

Strategy	Specific plan	ASR [Ω/cm <sup>2</sup> ]	CCD [mA/cm <sup>2</sup> ]	Ref.
Removal of Li <sub>2</sub> CO <sub>3</sub>	Reacting GE with carbon	28	-	[34]
Removal of Li <sub>2</sub> CO <sub>3</sub>	Heating GE	178	-	[35]
Removal of Li <sub>2</sub> CO <sub>3</sub>	HCl treatment	26	-	[36]
Removal of Li <sub>2</sub> CO <sub>3</sub>	H <sub>3</sub> PO <sub>4</sub> treatment	7	0.8	[37]
Alloy interlayers	Al <sub>2</sub> O <sub>3</sub>	1	-	[38]
Alloy interlayers	Cu <sub>3</sub> Sn <sub>3</sub>	236	-	[47]
Alloy interlayers	Cu/Li <sub>3</sub> N	83.4	1.2	[33]
Alloy interlayers	Low graphitized carbon	9	1.2	[53]
Alloy interlayers	MoS <sub>2</sub>	14	2.2	[55]
Soft interlayers	PVDF-HFP-based GPE	214	-	[56a]
Soft interlayers	LP30 liquid electrolyte	580	-	[57]
Soft interlayers	PIN@SN	104	-	[61]
Design of metal anodes	Li-C	11	1	[64]
Design of metal anodes	Li <sub>3</sub> N added	11	1.5	[66]
Design of metal anodes	Li-C	7	10	[67a]
Design of metal anodes	Molten Li	0.4	-	[68b]
Changes of GEs	High-temperature calcination	49	-	[77]
Changes of GEs	Coating LiAlO <sub>2</sub>	25	0.75	[31a]
Changes of GEs	Coating and infusing Li <sub>3</sub> PO <sub>4</sub>	1	2.2	[79]

standing the underlying reasons, and further providing theoretical guidance for future studies. Moreover, pre-screening with simulations before the experiment can greatly improve research efficiency and avoid unnecessary waste.

- 4) From a practical point of view, the costs of interfacial modifications cannot be ignored. Therefore, raw materials costs, devices costs and time costs should all be taken into consideration. For example, most of the metal or nonmetal reagents required to synthesize the alloy interlayers and the supporting devices like ALD are expensive, and the process is time-consuming. But, ALD can accurately control the thickness to get nanometer-scale interlayer, and facilitate large-scale manufacturing which is beneficial for reducing cost. Notably, up to now, all the proposed strategies can only be performed at a laboratory level due to the low yield and harsh conditions. For long-term development, great efforts focused on this issue are highly required.

## Acknowledgements

This work was financially supported by the Strategic Priority Research Program of the Chinese Academy of Sciences (XDA21010210), the National Key R&D Program of China (2016YFB0100103), the National Natural Science Foundation of China (21725103 and 21905269), the Jilin Province Science and Technology Development Plan Funding Project (20180101203JC, 20200201079JC), the Jilin Province Capital Construction Funds Project (2020 C026-1), and Changchun Science and Technology Development Plan Funding Project (19SS010).

## Conflict of Interest

The authors declare no conflict of interest.

**Keywords:** dendrite · garnet electrolyte · interface · Li metal · resistance · solid-state electrolyte

- [1] C. Wang, A. Wang, L. Ren, X. Guan, D. Wang, A. Dong, C. Zhang, G. Li, J. Luo, *Adv. Funct. Mater.* **2019**, *29*, 1905940.
- [2] A. Manthiram, X. Yu, S. Wang, *Nat. Rev. Mater.* **2017**, *2*, 16103.
- [3] T. Famprikis, P. Canepa, J. A. Dawson, M. S. Islam, C. Masquelier, *Nat. Mater.* **2019**, *18*, 1278–1291.
- [4] X. Wang, R. Kerr, F. Chen, N. Goujon, J. M. Pringle, D. Mecerreyes, M. Forsyth, P. C. Howlett, *Adv. Mater.*, DOI: 10.1002/adma.201905219.
- [5] a) R. Murugan, V. Thangadurai, W. Weppner, *Angew. Chem. Int. Ed.* **2007**, *46*, 7778–7781; b) C. Ma, Y. Cheng, K. Yin, J. Luo, A. Sharafi, J. Sakamoto, J. Li, K. L. More, N. J. Dudney, M. Chi, *Nano Lett.* **2016**, *16*, 7030–7036; c) Q. Liu, Z. Geng, C. Han, Y. Fu, S. Li, Y. He, F. Kang, B. Li, *J. Power Sources* **2018**, *389*, 120–134.
- [6] a) X. Huang, Y. Lu, H. Guo, Z. Song, T. Xiu, M. E. Badding, Z. Wen, *ACS Appl. Energy Mater.* **2018**, *1*, 5355–5365; b) S. Narayanan, F. Ramezani-pour, V. Thangadurai, *Inorg. Chem.* **2015**, *54*, 6968–6977; c) G. Han, B. Kinzer, R. Garcia-Mendez, H. Choe, J. Wolfenstine, J. Sakamoto, *J. Eur. Ceram. Soc.* **2020**, *40*, 1999–2006.
- [7] A. J. Samson, K. Hofstetter, S. Bag, V. Thangadurai, *Energy Environ. Sci.* **2019**, *12*, 2957–2975.
- [8] Z. Shen, W. Zhang, G. Zhu, Y. Huang, Q. Feng, Y. Lu, *Small Methods* **2019**, *4*, 1900592.
- [9] F. Han, Y. Zhu, X. He, Y. Mo, C. Wang, *Adv. Energy Mater.* **2016**, *6*, 1501590.
- [10] Y. Zhu, J. G. Connell, S. Tepavcevic, P. Zapol, R. Garcia-Mendez, N. J. Taylor, J. Sakamoto, B. J. Ingram, L. A. Curtiss, J. W. Freeland, D. D. Fong, N. M. Markovic, *Adv. Energy Mater.* **2019**, *9*, 1803440.
- [11] H. Zheng, S. Wu, R. Tian, Z. Xu, H. Zhu, H. Duan, H. Liu, *Adv. Funct. Mater.* **2019**, *30*, 1906189.
- [12] L. Cheng, E. J. Crumlin, W. Chen, R. Qiao, H. Hou, F. S. Lux, V. Zorba, R. Russo, R. Kostecki, Z. Liu, K. Persson, W. Yang, J. Cabana, T. Richardson, G. Chen, M. Doeff, *Phys. Chem. Chem. Phys.* **2014**, *16*, 18294–18300.
- [13] A. Sharafi, S. Yu, M. Naguib, M. Lee, C. Ma, H. M. Meyer, J. Nanda, M. Chi, D. J. Siegel, J. Sakamoto, *J. Mater. Chem. A* **2017**, *5*, 13475–13487.
- [14] W. Xia, B. Xu, H. Duan, X. Tang, Y. Guo, H. Kang, H. Li, H. Liu, *J. Am. Ceram. Soc.* **2017**, *100*, 2832–2839.
- [15] a) Y. Jin, P. J. McGinn, *J. Power Sources* **2013**, *239*, 326–331; b) R. H. Brugge, A. K. O. Hekselman, A. Cavallaro, F. M. Pesci, R. J. Chater, J. A. Kilner, A. Aguadero, *Chem. Mater.* **2018**, *30*, 3704–3713.
- [16] W. Xia, B. Xu, H. Duan, Y. Guo, H. Kang, H. Li, H. Liu, *ACS Appl. Mater. Interfaces* **2016**, *8*, 5335–5342.
- [17] C. Monroe, J. Newman, *J. Electrochem. Soc.* **2005**, *152*, A396–A404.
- [18] S. Yu, R. D. Schmidt, R. Garcia-Mendez, E. Herbert, N. J. Dudney, J. B. Wolfenstine, J. Sakamoto, D. J. Siegel, *Chem. Mater.* **2015**, *28*, 197–206.
- [19] a) C. Wang, Y. Gong, J. Dai, L. Zhang, H. Xie, G. Pastel, B. Liu, E. Wachsman, H. Wang, L. Hu, *J. Am. Chem. Soc.* **2017**, *139*, 14257–14264; b) R. Raj, J. Wolfenstine, *J. Power Sources* **2017**, *343*, 119–126; c) S. Yu, D. J. Siegel, *ACS Appl. Mater. Interfaces* **2018**, *10*, 38151–38158.
- [20] M. J. Wang, R. Choudhury, J. Sakamoto, *Joule* **2019**, *3*, 2165–2178.
- [21] T. Krauskopf, H. Hartmann, W. G. Zeier, J. Janek, *ACS Appl. Mater. Interfaces* **2019**, *11*, 14463–14477.
- [22] a) W. S. LePage, Y. Chen, E. Kazyak, K.-H. Chen, A. J. Sanchez, A. Poli, E. M. Arruda, M. D. Thouless, N. P. Dasgupta, *J. Electrochem. Soc.* **2019**, *166*, A89–A97; b) T. Krauskopf, B. Mogwitz, C. Rosenbach, W. G. Zeier, J. Janek, *Adv. Energy Mater.* **2019**, *9*, 1902568; c) A. Sharafi, H. M. Meyer, J. Nanda, J. Wolfenstine, J. Sakamoto, *J. Power Sources* **2016**, *302*, 135–139.
- [23] T. Krauskopf, R. Dippel, H. Hartmann, K. Peppler, B. Mogwitz, F. H. Richter, W. G. Zeier, J. Janek, *Joule* **2019**, *3*, 2030–2049.
- [24] a) W. Manalastas, J. Rikarte, R. J. Chater, R. Brugge, A. Aguadero, L. Buannic, A. Llordés, F. Aguesse, J. Kilner, *J. Power Sources* **2019**, *412*, 287–293; b) L. Porz, T. Swamy, B. W. Sheldon, D. Rettenwander, T. Frömling, H. L. Thaman, S. Berendts, R. Uecker, W. C. Carter, Y.-M. Chiang, *Adv. Energy Mater.* **2017**, *7*, 1701003; c) S. Kim, C. Jung, H. Kim, K. E. Thomas-Alyea, G. Yoon, B. Kim, M. E. Badding, Z. Song, J. Chang, J. Kim, D. Im, K. Kang, *Adv. Energy Mater.*, DOI: 10.1002/aenm.201903993.
- [25] G. Bucci, J. Christensen, *J. Power Sources* **2019**, *441*, 227186.
- [26] Y. Ren, Y. Shen, Y. Lin, C. W. Nan, *ACS Appl. Mater. Interfaces* **2019**, *11*, 5928–5937.
- [27] E. J. Cheng, A. Sharafi, J. Sakamoto, *Electrochim. Acta* **2017**, *223*, 85–91.
- [28] C. L. Tsai, V. Roddatis, C. V. Chandran, Q. Ma, S. Uhlenbruck, M. Bram, P. Heitjans, O. Guillon, *ACS Appl. Mater. Interfaces* **2016**, *8*, 10617–10626.
- [29] a) B. Dong, S. R. Yeandel, P. Goddard, P. R. Slater, *Chem. Mater.* **2019**, *32*, 215–223; b) Z. Zhang, A. R. Gonzalez, K. L. Choy, *ACS Appl. Energy Mater.* **2019**, *2*, 7438–7448.
- [30] S. Smetaczek, A. Wachter-Welzl, R. Wagner, D. Rettenwander, G. Amthauer, L. Andrejs, S. Taibl, A. Limbeck, J. Fleig, *J. Mater. Chem. A* **2019**, *7*, 6818–6831.
- [31] a) Y. Song, L. Yang, W. Zhao, Z. Wang, Y. Zhao, Z. Wang, Q. Zhao, H. Liu, F. Pan, *Adv. Energy Mater.* **2019**, *9*, 1900671; b) F. Aguesse, W. Manalastas, L. Buannic, J. M. L. D. Amo, G. P. D. Silva, R. Mücke, J. Kilner, *ACS Appl. Mater. Interfaces* **2017**, *9*, 3808–3816; c) Y. Ren, Y. Shen, Y. Lin, C.-W. Nan, *Electrochem. Commun.* **2015**, *57*, 27–30.
- [32] H.-K. Tian, B. Xu, Y. Qi, *J. Power Sources* **2018**, *392*, 79–86.
- [33] H. Huo, Y. Chen, R. Li, N. Zhao, J. Luo, J. G. P. D. Silva, R. Mücke, P. Kaghazchi, X. Guo, X. Sun, *Energy Environ. Sci.* **2020**, *13*, 127–134.
- [34] Y. Li, X. Chen, A. Dolocan, Z. Cui, S. Xin, L. Xue, H. Xu, K. Park, J. B. Goodenough, *J. Am. Chem. Soc.* **2018**, *140*, 6448–6455.
- [35] L. Cheng, M. Liu, A. Mehta, H. Xin, F. Lin, K. Persson, G. Chen, E. J. Crumlin, M. Doeff, *ACS Appl. Energy Mater.* **2018**, *1*, 7244–7252.
- [36] H. Huo, Y. Chen, N. Zhao, X. Lin, J. Luo, X. Yang, Y. Liu, X. Guo, X. Sun, *Nano Energy* **2019**, *61*, 119–125.
- [37] Y. Ruan, Y. Lu, X. Huang, J. Su, C. Sun, J. Jin, Z. Wen, *J. Mater. Chem. A* **2019**, *7*, 14565–14574.

- [38] X. Han, Y. Gong, K. K. Fu, X. He, G. T. Hitz, J. Dai, A. Pearce, B. Liu, H. Wang, G. Rubloff, Y. Mo, V. Thangadurai, E. D. Wachsman, L. Hu, *Nat. Mater.* **2017**, *16*, 572–579.
- [39] W. Luo, Y. Gong, Y. Zhu, K. K. Fu, J. Dai, S. D. Lacey, C. Wang, B. Liu, X. Han, Y. Mo, E. D. Wachsman, L. Hu, *J. Am. Chem. Soc.* **2016**, *138*, 12258–12262.
- [40] K. K. Fu, Y. Gong, Z. Fu, H. Xie, Y. Yao, B. Liu, M. Carter, E. Wachsman, L. Hu, *Angew. Chem. Int. Ed.* **2017**, *56*, 14942–14947.
- [41] W. Luo, Y. Gong, Y. Zhu, Y. Li, Y. Yao, Y. Zhang, K. K. Fu, G. Pastel, C. F. Lin, Y. Mo, E. D. Wachsman, L. Hu, *Adv. Mater.* **2017**, *29*, 1606042.
- [42] C. Wang, Y. Gong, B. Liu, K. Fu, Y. Yao, E. Hitz, Y. Li, J. Dai, S. Xu, W. Luo, E. D. Wachsman, L. Hu, *Nano Lett.* **2017**, *17*, 565–571.
- [43] W. Feng, X. Dong, P. Li, Y. Wang, Y. Xia, *J. Power Sources* **2019**, *419*, 91–98.
- [44] J. Lou, G. Wang, Y. Xia, C. Liang, H. Huang, Y. Gan, X. Tao, J. Zhang, W. Zhang, *J. Power Sources* **2020**, *448*, 227440.
- [45] a) Y. Shao, H. Wang, Z. Gong, D. Wang, B. Zheng, J. Zhu, Y. Lu, Y.-S. Hu, X. Guo, H. Li, X. Huang, Y. Yang, C.-W. Nan, L. Chen, *ACS Energy Lett.* **2018**, *3*, 1212–1218; b) C. Zhou, A. J. Samson, K. Hofstetter, V. Thangadurai, *Sustainable Energy Fuels* **2018**, *2*, 2165–2170; c) M. Cai, Y. Lu, J. Su, Y. Ruan, C. Chen, B. V. R. Chowdari, Z. Wen, *ACS Appl. Mater. Interfaces* **2019**, *11*, 35030–35038; d) B. Sun, Y. Jin, J. Lang, K. Liu, M. Fang, H. Wu, *Chem. Commun.* **2019**, *55*, 6704–6707.
- [46] a) M. He, Z. Cui, C. Chen, Y. Li, X. Guo, *J. Mater. Chem. A* **2018**, *6*, 11463–11470; b) H. Koshikawa, S. Matsuda, K. Kamiya, M. Miyayama, Y. Kubo, K. Uosaki, K. Hashimoto, S. Nakanishi, *J. Electroanal. Chem.* **2019**, *835*, 143–149.
- [47] W. Feng, X. Dong, Z. Lai, X. Zhang, Y. Wang, C. Wang, J. Luo, Y. Xia, *ACS Energy Lett.* **2019**, *4*, 1725–1731.
- [48] a) K. Liu, R. Zhang, M. Wu, H. Jiang, T. Zhao, *J. Power Sources* **2019**, *433*, 226691; b) Y. Chen, M. He, N. Zhao, J. Fu, H. Huo, T. Zhang, Y. Li, F. Xu, X. Guo, *J. Power Sources* **2019**, *420*, 15–21.
- [49] B. Hu, W. Yu, B. Xu, X. Zhang, T. Liu, Y. Shen, Y. H. Lin, C. W. Nan, L. Li, *ACS Appl. Mater. Interfaces* **2019**, *11*, 34939–34947.
- [50] G. V. Alexandrov, M. S. Indu, S. Kamakshy, R. Murugan, *Electrochim. Acta* **2020**, *332*, 135511.
- [51] H. Xu, Y. Li, A. Zhou, N. Wu, S. Xin, Z. Li, J. B. Goodenough, *Nano Lett.* **2018**, *18*, 7414–7418.
- [52] N. Zhao, R. Fang, M.-H. He, C. Chen, Y.-Q. Li, Z.-J. Bi, X.-X. Guo, *Rare Met.* **2018**, *37*, 473–479.
- [53] W. Feng, X. Dong, X. Zhang, Z. Lai, P. Li, C. Wang, Y. Wang, Y. Xia, *Angew. Chem. Int. Ed.* **2020**, *59*, 5346–5349.
- [54] C. Chen, Q. Li, Y. Li, Z. Cui, X. Guo, H. Li, *ACS Appl. Mater. Interfaces* **2018**, *10*, 2185–2190.
- [55] J. Fu, P. Yu, N. Zhang, G. Ren, S. Zheng, W. Huang, X. Long, H. Li, X. Liu, *Energy Environ. Sci.* **2019**, *12*, 1404–1412.
- [56] a) B. Liu, Y. Gong, K. Fu, X. Han, Y. Yao, G. Pastel, C. Yang, H. Xie, E. D. Wachsman, L. Hu, *ACS Appl. Mater. Interfaces* **2017**, *9*, 18809–18815; b) J. Wang, Y. Yin, T. Liu, X. Yang, Z. Chang, X. Zhang, *Nano Res.* **2018**, *11*, 3434–3441.
- [57] J. Liu, X. Gao, G. O. Hartley, G. J. Rees, C. Gong, F. H. Richter, J. Janek, Y. Xia, A. W. Robertson, L. R. Johnson, P. G. Bruce, *Joule* **2020**, *4*, 101–108.
- [58] B. Xu, H. Duan, H. Liu, C. A. Wang, S. Zhong, *ACS Appl. Mater. Interfaces* **2017**, *9*, 21077–21082.
- [59] H. Duan, Y. X. Yin, Y. Shi, P. F. Wang, X. D. Zhang, C. P. Yang, J. L. Shi, R. Wen, Y. G. Guo, L. J. Wan, *J. Am. Chem. Soc.* **2018**, *140*, 82–85.
- [60] a) L. Chen, Z. Huang, W. Pang, Z. Jin, Y. Li, C.-A. Wang, *Electrochim. Acta* **2020**, *330*, 135352; b) S. A. Pervez, P. Ganjeh-Anzabi, U. Farooq, M. Trifkovic, E. P. L. Roberts, V. Thangadurai, *Adv. Mater. Interfaces* **2019**, *6*, 1900186; c) H. Huo, Y. Chen, J. Luo, X. Yang, X. Guo, X. Sun, *Adv. Energy Mater.* **2019**, *9*, 1804004.
- [61] D. Dong, B. Zhou, Y. Sun, H. Zhang, G. Zhong, Q. Dong, F. Fu, H. Qian, Z. Lin, D. Lu, Y. Shen, J. Wu, L. Chen, H. Chen, *Nano Lett.* **2019**, *19*, 2343–2349.
- [62] C. Wang, H. Xie, L. Zhang, Y. Gong, G. Pastel, J. Dai, B. Liu, E. D. Wachsman, L. Hu, *Adv. Energy Mater.* **2018**, *8*, 1701963.
- [63] Y. Lu, X. Huang, Y. Ruan, Q. Wang, R. Kun, J. Yang, Z. Wen, *J. Mater. Chem. A* **2018**, *6*, 18853–18858.
- [64] J. Duan, W. Wu, A. M. Nolan, T. Wang, J. Wen, C. Hu, Y. Mo, W. Luo, Y. Huang, *Adv. Mater.* **2019**, *31*, e1807243.
- [65] C. Yang, H. Xie, W. Ping, K. Fu, B. Liu, J. Rao, J. Dai, C. Wang, G. Pastel, L. Hu, *Adv. Mater.* **2019**, *31*, e1804815.
- [66] Y. Huang, B. Chen, J. Duan, F. Yang, T. Wang, Z. Wang, W. Yang, C. Hu, W. Luo, Y. Huang, *Angew. Chem. Int. Ed.* **2020**, *59*, 3699–3704.
- [67] a) G. T. Hitz, D. W. McOwen, L. Zhang, Z. Ma, Z. Fu, Y. Wen, Y. Gong, J. Dai, T. R. Hamann, L. Hu, E. D. Wachsman, *Mater. Today* **2019**, *22*, 50–57; b) D. W. McOwen, S. Xu, Y. Gong, Y. Wen, G. L. Godbey, J. E. Gritton, T. R. Hamann, J. Dai, G. T. Hitz, L. Hu, E. D. Wachsman, *Adv. Mater.* **2018**, *30*, e1707132; c) C. Yang, L. Zhang, B. Liu, S. Xu, T. Hamann, D. McOwen, J. Dai, W. Luo, Y. Gong, E. D. Wachsman, L. Hu, *Proc. Natl. Acad. Sci. USA* **2018**, *115*, 3770–3775.
- [68] a) Y. Jin, K. Liu, J. Lang, X. Jiang, Z. Zheng, Q. Su, Z. Huang, Y. Long, C. Wang, H. Wu, Y. Cui, *Joule* **2020**, *4*, 262–274; b) Y. Jin, K. Liu, J. Lang, D. Zhuo, Z. Huang, C. A. Wang, H. Wu, Y. Cui, *Nat. Energy* **2018**, *3*, 732–738.
- [69] C.-Z. Zhao, Q. Zhang, *Joule* **2019**, *3*, 1575–1577.
- [70] S. Li, H. Wang, J. Cuthbert, T. Liu, J. F. Whitacre, K. Matyjaszewski, *Joule* **2019**, *3*, 1637–1646.
- [71] a) J. Gai, E. Zhao, F. Ma, D. Sun, X. Ma, Y. Jin, Q. Wu, Y. Cui, *J. Eur. Ceram. Soc.* **2018**, *38*, 1673–1678; b) F. M. Pesci, R. H. Brugge, A. K. O. Hekselman, A. Cavallaro, R. J. Chater, A. Aguiadero, *J. Mater. Chem. A* **2018**, *6*, 19817–19827.
- [72] a) M. Yi, T. Liu, X. Wang, J. Li, C. Wang, Y. Mo, *Ceram. Int.* **2019**, *45*, 786–792; b) X. Zeng, A. J. Martinolich, K. A. See, K. T. Faber, *J. Energy Storage* **2020**, *27*, 101128.
- [73] a) J. Su, X. Huang, Z. Song, T. Xiu, M. E. Badding, J. Jin, Z. Wen, *Ceram. Int.* **2019**, *45*, 14991–14996; b) M. B. Dixit, M. Regala, F. Shen, X. Xiao, K. B. Hatzell, *ACS Appl. Mater. Interfaces* **2019**, *11*, 2022–2030.
- [74] a) H. Xie, C. Li, W. H. Kan, M. Avdeev, C. Zhu, Z. Zhao, X. Chu, D. Mu, F. Wu, *J. Mater. Chem. A* **2019**, *7*, 20633–20639; b) W. Zhang, C. Sun, *J. Phys. Chem. Solids* **2019**, *135*, 109080; c) R. H. Basappa, T. Ito, T. Morimura, R. Bekarevich, K. Mitsuishi, H. Yamada, *J. Power Sources* **2017**, *363*, 145–152.
- [75] S. P. Kammampata, R. H. Basappa, T. Ito, H. Yamada, V. Thangadurai, *ACS Appl. Energy Mater.* **2019**, *2*, 1765–1773.
- [76] Y. Li, B. Xu, H. Xu, H. Duan, X. Lu, S. Xin, W. Zhou, L. Xue, G. Fu, A. Manthiram, J. B. Goodenough, *Angew. Chem. Int. Ed.* **2017**, *56*, 753–756.
- [77] J. F. Wu, B. W. Pu, D. Wang, S. Q. Shi, N. Zhao, X. Guo, X. Guo, *ACS Appl. Mater. Interfaces* **2019**, *11*, 898–905.
- [78] B. Xu, W. Li, H. Duan, H. Wang, Y. Guo, H. Li, H. Liu, *J. Power Sources* **2017**, *354*, 68–73.
- [79] T. Deng, X. Ji, Y. Zhao, L. S. Cao, S. Li, S. Hwang, C. Luo, P. F. Wang, H. P. Jia, X. L. Fan, X. C. Lu, D. Su, X. L. Sun, C. S. Wang, J. G. Zhang, *Adv. Mater.*, DOI: 10.1002/adma.202000030.

Manuscript received: April 9, 2020

Revised manuscript received: May 21, 2020

Accepted manuscript online: June 15, 2020

Version of record online: July 8, 2020